applied sciences

MDPI

Article

Cortical Connectivity Response to Hyperventilation in Focal Epilepsy: A Stereo-EEG Study

Lorenzo Ferri [1,2,†], Federico Mason [2,3,†], Lidia Di Vito [1], Elena Pasini [1], Roberto Michelucci [1], Francesco Cardinale [4,5], Roberto Mai [4], Lara Alvisi [1,2], Luca Zanuttini [2], Matteo Martinoni [1,*] and Francesca Bisulli [1,2]

1 IRCCS Istituto delle Scienze Neurologiche di Bologna, Full Member of the European Reference Network EpiCARE, 40139 Bologna, Italy; lorenzo.ferri@ausl.bologna.it (L.F.); lidia.divito@ausl.bologna.it (L.D.V.); elena.pasini@isnb.it (E.P.); roberto.michelucci@isnb.it (R.M.); lara.alvisi@unibo.it (L.A.); francesca.bisulli@unibo.it (F.B.)
2 Department of Neuromotor and Biomedical Sciences, University of Bologna, 40127 Bologna, Italy; federico.mason@unipd.it (F.M.); luca.zanuttini@studio.unibo.it (L.Z.)
3 Department of Information Engineering, University of Padova, 35131 Padova, Italy
4 Centro Munari Chirurgia dell'Epilessia e del Parkinson, Niguarda Hospital, 20162 Milan, Italy; francesco.cardinale@ospedaleniguarda.it (F.C.); roberto.mai@ospedaleniguarda.it (R.M.)
5 Unit of Neuroscience, Department of Medicine and Surgery, University of Parma, 43124 Parma, Italy
* Correspondence: m.martinoni@isnb.it
† These authors contributed equally to this work.

Abstract: Hyperventilation (HV) is an activation technique performed during clinical practices to trigger epileptiform activities, supporting the neurophysiological evaluation of patients with epilepsy. Although the role of HV has often been questioned, especially in the case of focal epilepsy, no studies have ever assessed how cortical structures respond to such a maneuver via intracranial EEG recordings. This work aims to fill this gap by evaluating the HV effects on the Stereo-EEG (SEEG) signals from a cohort of 10 patients with drug-resistant focal epilepsy. We extracted multiple quantitative metrics from the SEEG signals and compared the results obtained during HV, awake status, non-REM sleep, and seizure onset. Our findings show that the cortical connectivity, estimated via the phase transfer entropy (PTE) algorithm, strongly increases during the HV maneuver, similar to non-REM sleep. The opposite effect is observed during seizure onset, as ictal transitions involve the desynchronization of the brain structures within the epileptogenic zone. We conclude that HV promotes a conductive environment that may facilitate the propagation of epileptiform activities but is not sufficient to trigger seizures in focal epilepsy.

Keywords: stereoelectroencephalography; focal epilepsy; hyperventilation; brain dynamics; network analysis; phase transfer entropy

Citation: Ferri, L.; Mason, F.; Di Vito, L.; Pasini E.; Michelucci R.; Cardinale F.; Mai R.; Alvisi L.; Zanuttini L.; Martinoni M. Bisulli F,. Cortical Connectivity Response to Hyperventilation in Focal Epilepsy: A Stereo-EEG Study. *Appl. Sci.* **2024**, *14*, 8494. https://doi.org/10.3390/app14188494

Academic Editor: Alexander N. Pisarchik

Received: 30 August 2024
Revised: 16 September 2024
Accepted: 19 September 2024
Published: 20 September 2024

1. Introduction

Hyperventilation (HV) is a well-known activation technique performed during routine Electroencephalography (EEG) recording, recommended by the international guideline of the main clinical neuro-physiology and epilepsy societies [1]. In practice, HV involves deep and regular breathing at a rate of approximately 20 breaths per minute for a duration of 2 to 4 min. This technique was introduced in clinical practice by Otfrid Foerster who, in 1925, observed that HV could trigger *latent epilepsy* [2]. After the broad diffusion of EEG, HV became one of the most common procedures to elicit epileptic activities, offering valuable information for the medical management of epilepsy [3].

In the past years, several studies have demonstrated that the main HV effect is a physiological slowing of background EEG activity. Particularly, in people with epilepsy, it has been observed that HV could increase focal and generalized Interictal Epileptiform

Discharges (IEDs) [4]. A possible explanation for such a phenomenon relies on the vasoconstriction associated with cerebral hypoxia and the intracellular pH increment associated with respiratory hypocapnia. More specifically, it has been shown that cerebral hypoxia induces a negative DC shift variation over the EEG signal [5], while respiratory hypocapnia leads to higher excitatory postsynaptic potentials [6]. On the other hand, other studies have hypothesized that the cortical response to HV is due to sympathetic over-activation, which is notoriously considered a seizure trigger in temporal lobe epilepsy [7].

The effectiveness of HV is well established in generalized epilepsy: in the case of absence seizures, it has been demonstrated that HV generates a spike-and-wave complex in over 90% of the cases and triggers clinical seizures in around 50% of the cases [8]. On the other hand, there is limited agreement regarding the role of HV as an activation maneuver in focal epilepsy, especially in adults, who, notably, also present less significant autonomic abnormalities compared to the pediatric population [9]. A study carried out on a large patient cohort demonstrated that HV rarely triggers clinical seizures or increases the IED frequency [10]. However, other authors found that temporal lobe epilepsy might be more sensitive to HV than other types of epilepsy, suggesting its potential role in shortening presurgical evaluations [11].

A deeper comprehension of HV effects could be offered by using quantitative approaches for analyzing cortical or scalp EEG signals. In this context, the naive approach consists of analyzing the recorded signals in the time–frequency domain, evaluating the energy spectral density and the distribution of the signal phase. Other approaches aim to estimate the interdependency within different signals, considering connectivity-based metrics, which have proven to be extremely valuable for detecting epileptiform activities or discerning different populations [12]. Interestingly, most recent connectivity techniques focus on the analysis of the phase distribution of the EEG signals, using algorithms such as the Phase Locking Value (PLV), the Phase Lag Index (PLI), or the Phase Transfer Entropy (PTE) [13]. The latter algorithm combines the analysis of the signal instantaneous phase with the Granger causality and enables the estimation of the effective relations between signals generated by different brain structures [14].

A recent study concluded that HV increases the magnitude of the EEG power spectra, especially in the cingulate cortex, and demonstrated that different brain regions respond differently to respiratory hypocapnia [15]. The same study denoted how HV leads to a higher increase in cortical connectivity in people with epilepsy than in healthy individuals. Nevertheless, quantitative analysis of EEG traces during HV is scarce in the current literature, and it is still unclear how HV impacts the epileptogenic network. A better understanding of the relation between HV and seizure development could be offered by the analysis of intracranial EEG recording as allowed by Stereo-EEG (SEEG). This latter is an invasive surgical procedure that enables the recording of deep cortical signals, providing fundamental information for the accurate localization of the Epileptogenic Zone (EZ), i.e., the cortex area responsible for seizure generation [16].

To our knowledge, at the present time, there have been no research works investigating the HV mechanisms by exploiting the intracranial EEG signals. This study aimed to fill this gap and assess how the HV affects cortical brain structures in patients with focal epilepsy. Our fundamental hypothesis is that HV promotes an increase in cortical connectivity as occurs during the Non-REM sleep (N-REM) status, but such an effect is not directly associated with the outbreak of the seizure onset. To achieve this goal, we selected a cohort of focal epilepsy patients that underwent SEEG monitoring for pre-surgical evaluation. Then, we computed multiple quantitative metrics from the recorded signals, using the PTE algorithm to estimate cortical connectivity. To spotlight the HV effects, we compared the SEEG signals associated with HV against those associated with the awake status, N-REM, and ictal transition, i.e., the period during which the seizure starts to form.

2. Materials

This study considered a cohort of 10 *consecutive patients* that underwent SEEG monitoring at IRCCS Institute of Neurological Sciences of Bologna from January 2022 to June 2024. The study protocol was approved by the local ethics committee (protocol number 89-2021, committee code 20230), and written informed consent was obtained from each patient. The SEEG implants included multiple electrodes, each presenting 5–18 recording sites, named *contacts*; the number and location of the electrodes were patient tailored, depending on the EZ localization hypothesis [17]. Each contact was 2.2 mm in length and was separated by 1.5 mm from neighboring contacts (Microdeep Intracerebral Electrodes-D08, Dixi Medical, Besançon, France).

The SEEG implantation followed the workflow developed at Niguarda Hospital and involved the construction of a multimodal scene of the patient's brain. The multimodal scenes made it possible for clinicians to comprehensively evaluate all the anatomical information regarding the cortical area explored by each contact [18]. The SEEG signals were recorded using the Nihon Kohden EEG 2100 (Tokyo, Japan), using a maximum of 256 channels, and a sampling frequency of $f_{\text{sampling}} = 1000$ Hz. To correlate electrical and clinical features, a high-definition synchronized video of each patient was recorded for the whole duration of the SEEG monitoring (up to 20 days per patient).

All patients underwent a standardized 1-hour-recording protocol during the second day of SEEG monitoring, which included two activation maneuvers, namely, HV and intermittent photic stimulation. Particularly, HV sessions consisted of a sequence of deep breaths, at a rate of approximately 20 breaths/minute, for a total period of 4 min. To ensure the correct progress of the maneuver, expert clinical personnel, normally a neurologist and a neurophysiological technician, were in charge of explaining the procedure to the patient and assisting him/her for the exam duration.

In this work, we excluded all the SEEG contacts exploring the White Matter (WM) since they have only a propagator function [19], focusing only on contacts exploring the Grey Matter (GM). The discrimination between WM and GM, as well as the selection of the SEEG epochs, was performed by a board-certified neurophysiologist (L.F.). No other SEEG channel was excluded from the analysis, making our methodology agnostic to the specific SEEG implant and the clinical and demographic features associated with each patient. Hence, a subset of 26 SEEG epochs per patient was selected for the analysis, according to the following specifics:

- One epoch associated with the *ictal transition*, namely the period that included the 20 s preceding and following the first ictal change;
- Five epochs associated with the HV maneuver;
- Ten epochs associated with recording periods during which the patient was awake;
- Ten epochs associated with recording periods during which the patient was asleep (N-REM phase).

Each epoch lasted $T_{\text{epoch}} = 40$ seconds, resulting in a multidimensional signal, whose components, named *channels*, described the electrical activity generated by the cortical sites explored by the SEEG implant. An example of the epochs is reported in Figure 1.

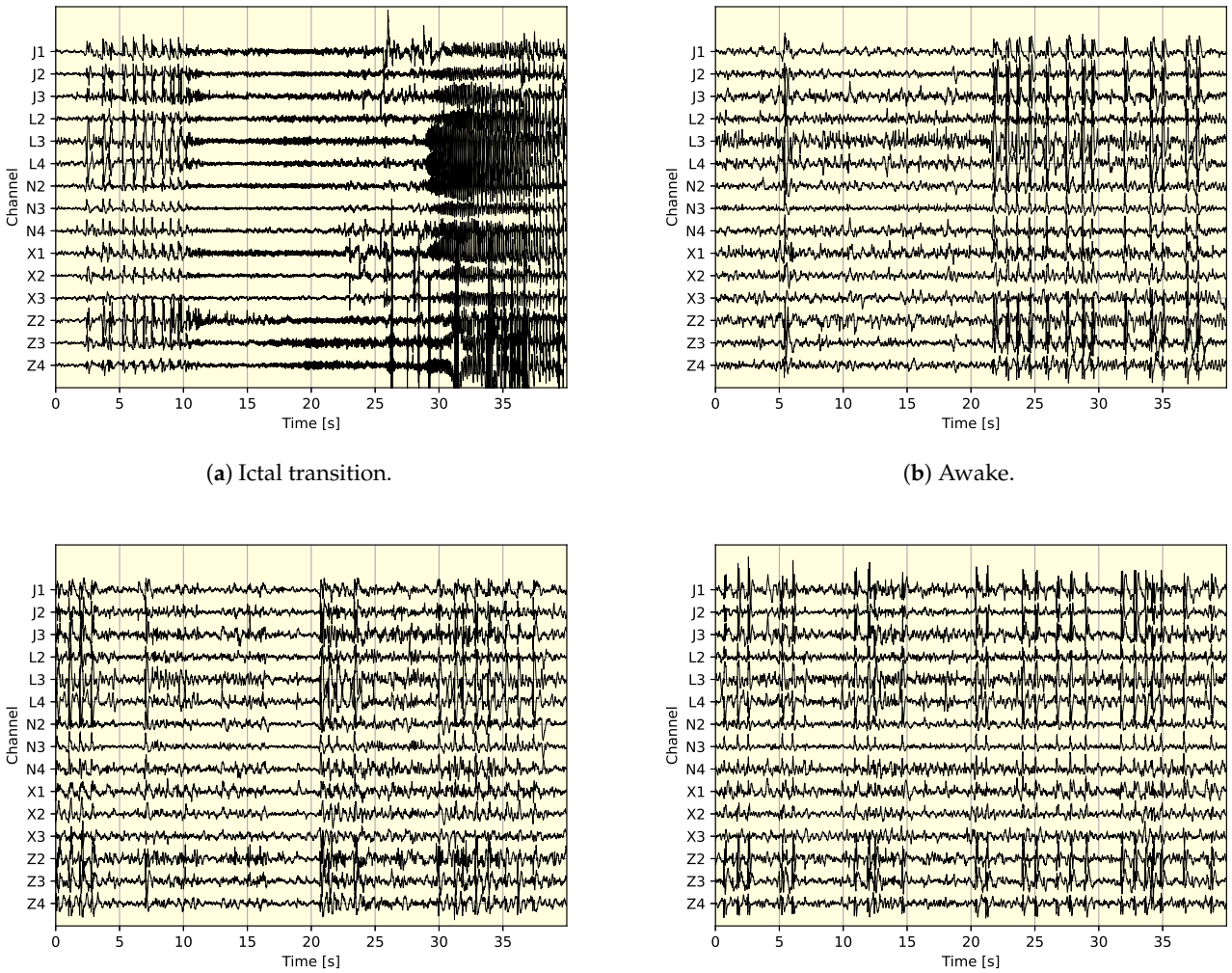

(**a**) Ictal transition.

(**b**) Awake.

(**c**) Non-REM sleep.

(**d**) Hyperventilation.

Figure 1. Example of SEEG epochs associated with one of the patients; the channels displayed are located within the EZ and are associated with marked epileptiform discharges; during the ictal transition, the epileptiform discharges evolve into low-voltage fast activities that trigger the epileptic seizure.

3. Methods

As a preliminary step, the SEEG epochs were processed by a *comb filter* to erase the powerline frequency f_{power} and its multiples $k \cdot f_{\text{power}}$, with $k \in \mathbb{Z}^+$, where $\mathbb{Z}^+$ represents the set of positive integers. Then, each channel was segmented into overlapping windows: the window duration was set to $T_{\text{window}} = 1.0$ s, and we inter-spaced consecutive windows by an interval $T_{\text{shift}} = 0.25$ s. Hence, each epoch was segmented in $W = \lfloor (T_{\text{signal}} - T_{\text{window}})/T_{\text{shift}} \rfloor = 156$ windows, where each window includes $n = T_{\text{window}} \cdot f_{\text{sampling}} = 1000$ samples. In the rest of the manuscript, we denote by $\mathcal{N}$ the set of channels within the same SEEG epoch and by $\mathcal{N}(t)$ the set of windows $x(t)$ lasting from time $t \cdot T_{\text{shift}}$ to time $t \cdot T_{\text{shift}} + T_{\text{window}}$, with $t \in \mathbb{Z}^+$. Therefore, a SEEG epoch including $N = |\mathcal{N}|$ channels was associated with a total of $N \cdot W$ windows.

3.1. Spectral Analysis

At first, we consider the Fourier Transform (FT) of the windows associated with each channel $x \in \mathcal{N}$ [20]. We write $\mathcal{X}(t)$ to indicate the FT of $x(t) \in \mathcal{N}(t)$: notably, $\mathcal{X}(t)$ includes $m = T_{\text{window}} \cdot f_{\text{sampling}}/2 = 500$ complex values, named *tones*, each associated

with a positive frequency $f \in B_{\text{total}} = [0, f_{\text{sampling}}/2]$. In particular, we can obtain the total energy $E_x(t)$ of $x(t)$ as

$$E_x(t) = \int_{B_{\text{total}}} \|\mathcal{X}(t,f)\|^2 df, \tag{1}$$

where $\|\cdot\|$ is the norm function and $\mathcal{X}(t,f)$ is the tone associated with frequency $f \in B_{\text{total}}$.

Given the Fourier representation of the signal, we study the relation between different frequency bands. Specifically, considering $B_{\text{low}} = [4, 30]$ Hz and $B_{\text{high}} = [30, 250]$ Hz as target bands, we compute the *energy ratio* $ER_x(t)$ of $x(t)$ as

$$ER_x(t) = \frac{\int_{B_{\text{high}}} \|\mathcal{X}(t,f)\|^2 df}{\int_{B_{\text{low}}} \|\mathcal{X}(t,f)\|^2 df}. \tag{2}$$

The value of $ER_x(t)$ increases whenever the channel x starts exhibiting fast oscillations, a phenomenon commonly associated with the onset of epileptic discharges [21].

Besides considering the magnitude of the FT, we also analyze the phase $\theta_x(t,f)$ of the different signal tones. Specifically, $\theta_x(t,f)$ represents the relative distances, measured in radians, between the starting time of window $x(t)$ and the peak amplitude of the Fourier sinusoid associated with frequency $f \in [0, f_{\text{sampling}}/2]$. In this work, we model the phase distribution $\theta_x(t)$ of $x(t)$ as a histogram, whose range is within $-\pi$ and $+\pi$, and whose bin number is chosen according to the *Sturges rule* [22]. Each bin $\vartheta \in \Theta$ includes a phase range lasting $2\pi/(log_2(m)+1)$ radians, where $m = 500$ is the number of Fourier tones associated with each window. Hence, we compute the entropy of $\theta_x(t)$ as

$$H(\theta_x(t)) = -\sum_{\vartheta \in \Theta} p_\vartheta(\theta_x(t)) \log(p_\vartheta(\theta_x(t))), \tag{3}$$

where $p_\vartheta(\theta_x(t))$ represents the probability that $\theta_x(t)$ takes values in the phase range associated with ϑ. Appreciably, $H(\theta_x(t))$ denotes the tendency of the FT of $x(t)$ to assume a large variety of phase values and is maximized when $\theta_x(t)$ is uniform. As $x(t)$ becomes more complex, it includes more sinusoidal components, leading to a higher entropy value [23].

3.2. Connectivity Analysis

Afterwards, we compute the Hilbert Transform (HT), obtaining the analytic representation $\mathcal{X}_a(t) = x(t) + HT(x(t))$ of each window $x(t) \in \mathcal{N}(t)$. The values $\mathcal{X}_a(t)$ are associated with an *instantaneous phase* $\phi_x(t,\tau)$, where τ is the time index of the window samples [24]. Also in this case, we model the instantaneous phase distribution $\phi_x(t)$ as a histogram, choosing the bin number according to the Sturges rule. Practically, each bin $\varphi \in \Phi$ includes a phase range lasting $2\pi/(log_2(n)+1)$ radians, where $n = 1000$ is the number of signal samples associated with each window. Hence, we compute the entropy of $\phi_x(t)$ as

$$H(\phi_x(t)) = -\sum_{\varphi \in \Phi} p_\varphi(\phi_x(t)) \log(p_\varphi(\phi_x(t))), \tag{4}$$

where $p_\varphi(\phi_x(t))$ represents the probability that $\phi_x(t)$ takes values in the phase range associated with φ. Despite being computed in different domains, $H(\phi_x(t))$ has a similar meaning to $H(\theta_x(t))$ and tends to increase as $x(t)$ obtains more complex patterns.

The instantaneous phase distribution is also used for describing the relations within the different channels $x \in \mathcal{N}$ in time [25]. To this goal, we consider the PTE algorithm, which, given a couple of channels $x, y \in \mathcal{N}$, estimates the influence that each of the channels exerts on the network [14]. The algorithm takes as input the instantaneous phase distribution $\phi_x(t)$ and $\phi_y(t)$ of $x(t)$ and $y(t)$ and estimates the amount of information in $\phi_x(t)$ that can

be used to predict the future evolution of $\phi_y(t)$. Specifically, the value of the PTE between $x(t)$ and $y(t)$, considering a lag δ, is obtained by

$$\begin{gathered} PTE_{x\to y}(t,\delta) = H\big(\phi_y(t), \phi_y(t+\tau)\big) + \\ H\big(\phi_x(t), \phi_y(t)\big) - H\big(\phi_x(t), \phi_y(t), \phi_y(t+\tau)\big) - H\big(\phi_y(t)\big), \end{gathered} \tag{5}$$

where $H(\cdot)$ denotes both the entropy and the mutual entropy function.

We recall that $PTE_{x\to y}(t,\delta)$ is an effective connectivity measure, which means that, in general, $PTE_{x\to y}(t,\delta) \neq PTE_{y\to x}(t,\tau)$ [26]. The value $PTE_{x\to y}(t,\delta)$ depends on the lag δ, i.e., the time distance at which the information transfer is estimated. To remove the dependency from δ, we redefine the PTE between $x(t)$ and $y(t)$ as the maximum value of $PTE_{x\to y}(t,\tau)$ among multiple lags:

$$PTE_{x\to y}(t) = \max_{\delta\in\{0,\ldots,\delta_{max}\}} PTE_{x\to y}(t,\tau), \tag{6}$$

where we set $\delta_{max} = 100$ ms. By doing so, the magnitude of the effective connection exerted on the channel y by the channel x at time t is given by $PTE_{x\to y}(t)$, while the propagation delay associated with such a connection is

$$\delta_{x\to y}(t) = \arg\max_{\delta\in\{0,\ldots,\delta_{max}\}} PTE_{x\to y}(t,\delta). \tag{7}$$

3.3. Statistical Analysis

We observe that all the measures are window-dependent and, thus, a series of $W = 156$ multiple measures is obtained for each epoch and measure. Hence, before performing the statistical analysis, we perform two additional steps. First, we normalize each measure by the average value observed during the epochs associated with the awake conditions. In this way, we implicitly assume that the awake epochs constitute a baseline condition, enabling a fair comparison between patients with different characteristics. Then, we compute the median ($Med[\cdot]$) and the interquartile range ($IQR[\cdot]$) of the measures obtained from each epoch, and consider such values to be the input information.

To assess if the SEEG epochs present significant differences according to the median or the interquartile range of any of the measures, we consider the *Welch's t-test*. The latter enables the comparison of the means of two data groups in case the variances are unknown and not equal [27]. Specifically, we perform a one-tailed test, checking whether the mean of a certain group of SEEG epochs is higher than another group, setting $\alpha = 0.05$ as the significance level. We recall that, by comparing the medians, we verify if a certain measure takes higher or lower values in a specific SEEG group with respect to another. Instead, by comparing the interquartile ranges, we assess if a measure takes more or less variable outcomes.

4. Results

The study included a total of 10 patients (6 Males), with a mean age of 37 years at the time of SEEG implantation. As shown in Table 1, it was possible to delineate an EZ that was located in the temporal lobe in seven patients, temporal–occipital cortex in two patients, and frontal in one patient. All the SEEG implants were unilateral (7 right, 3 left) and included 15 electrodes on average. In particular, four patients underwent temporo-parieto-occipital exploration, three fronto-temporal, two fronto-temporo-parietal, and one temporal. At the time of the study, six patients underwent epilepsy surgery, and the histopathological analysis revealed hippocampal sclerosis in four cases, focal cortical dysplasia in one case, and aspecific findings in the remaining one.

Table 1. Clinical and demographic characteristics of the studied population; F is for Frontal, T for Temporal, O for Occipital, THC for Thermocoagulation, ATL for Anterior Temporal Lobectomy, HS for Hippocampus Sclerosis, and FCD for Focal Cortical Dysplasia.

	Patient 1	**Patient 2**	**Patient 3**	**Patient 4**	**Patient 5**	**Patient 6**	**Patient 7**	**Patient 8**	**Patient 9**	**Patient 10**
Age (SEEG)	24	39	50	39	36	52	36	24	25	48
Sex	Male	Male	Female	Female	Male	Female	Male	Male	Female	Male
EZ localization	Left F	Left T	Left T	Right T-O	Right T-O	Right T	Left T	Right T	Right T	Right T
SEEG implant	Left F-T	Left F-T-P	Left F-T-P	Right T-P-O	Right T-P-O	Right F-T	Left T	Right T-P-O	Right T-P-O	Right F-T
Surgery	THC	THC + Left ATL	THC + Left ATL	THC	THC	THC + Right ATL	THC + Left ATL	THC	THC + Right ATL	THC + Right ATL
Histopathology	N/A	HS 1	HS 1	N/A	N/A	HS 1	FCD	N/A	Aspecific	HS 1

Our analysis focused on the following metrics: the energy ratio (ER), the entropy ($H(\theta)$) of the spectral phase distribution, and the Phase Transfer Entropy (PTE) computed from the instantaneous phase distribution. As shown in Table 2, both the ictal and awake periods presented higher energy ratio values than N-REM and awake periods. The energy ratio proved to be an effective biomarker for discerning HV activities from the N-REM conditions since it was sensibly lower when patients performed the HV maneuver. Taking the interquartile range into account, the differences are the same as those expressed in terms of median: in other words, the epochs presenting higher energy values are also associated with higher energy variability. Notably, there was slight evidence (p-value 0.09) that ictal transitions present more variable energy ratios than awake periods, although the latter showed higher median values for this metric (0.0672 vs. 0.0600).

Table 2. Comparison of the median and inter-quartile range of the energy ratio (ER) computed in different groups of SEEG epochs.

Metric	**Group 1**		**Group 2**		***p*-Value**	
	Label	**Mean ± CI**	**Label**	**Mean ± CI**	**Greater**	**Less**
$Med[ER]$	Ictal	0.0600 ± 0.0126	Awake	0.0672 ± 0.0207	0.2534	0.7466
	Ictal	0.0600 ± 0.0126	N-REM	0.0463 ± 0.0185	0.0587	0.9413
	Ictal	0.0600 ± 0.0126	HV	0.0277 ± 0.0077	0.0092	0.9908
	Awake	0.0672 ± 0.0207	N-REM	0.0463 ± 0.0185	0.0034	0.9966
	Awake	0.0672 ± 0.0207	HV	0.0277 ± 0.0077	<0.0001	>0.9999
	N-REM	0.0463 ± 0.0185	HV	0.0277 ± 0.0077	0.0066	0.9934
$IQR[ER]$	Ictal	0.0988 ± 0.0177	Awake	0.0849 ± 0.0192	0.0874	0.9126
	Ictal	0.0988 ± 0.0177	N-REM	0.0556 ± 0.0194	0.0185	0.9995
	Ictal	0.0988 ± 0.0177	HV	0.0382 ± 0.0115	0.0059	0.9941
	Awake	0.0849 ± 0.0192	N-REM	0.0556 ± 0.0194	0.0005	0.9995
	Awake	0.0849 ± 0.0192	HV	0.0382 ± 0.0115	<0.0001	>0.9999
	N-REM	0.0556 ± 0.0194	HV	0.0382 ± 0.0115	0.0181	0.9819

The entropy measures allowed us to differentiate between the ictal and the awake epochs from the N-REM and HV epochs (Table 3). At the same time, no significant difference was observed when comparing the ictal transition with the awake status, as well as the HV maneuver with the N-REM phase. Taking the interquartile range into account, the results followed an opposite trend compared to that before since higher entropy values were associated with lower entropy variability. The entropy during the ictal transition was slightly more variable (p-value of 0.063) than the one measured during the awake periods. In general, the variability was maximized during the ictal transition (with a value of 0.0988) and minimized during the HV (with a value of 0.0383).

Table 3. Comparison of the median and inter-quartile range of the spectral entropy ($H(\theta)$) computed in different groups of SEEG epochs.

Metric	Group 1		Group 2		*p*-Value	
	Label	Mean ± CI	Label	Mean ± CI	Greater	Less
$Med[H(\theta)]$	Ictal	1.8208 ± 0.0482	Awake	1.8350 ± 0.0445	0.6280	0.3720
	Ictal	1.8208 ± 0.0482	N-REM	1.7071 ± 0.0460	0.0038	0.9962
	Ictal	1.8208 ± 0.0482	HV	1.6903 ± 0.0307	0.0028	0.9972
	Awake	1.8350 ± 0.0445	N-REM	1.7071 ± 0.0460	<0.0001	>0.9999
	Awake	1.8350 ± 0.0445	HV	1.6903 ± 0.0307	0.0002	0.9998
	N-REM	1.7071 ± 0.0460	HV	1.6903 ± 0.0307	0.3287	0.6713
$IQR[H(\theta)]$	Ictal	0.5149 ± 0.0414	Awake	0.4726 ± 0.0464	0.0630	0.9370
	Ictal	0.5149 ± 0.0414	N-REM	0.5623 ± 0.0386	0.8126	0.1874
	Ictal	0.5149 ± 0.0414	HV	0.5975 ± 0.0125	0.9131	0.0869
	Awake	0.4726 ± 0.0464	N-REM	0.5623 ± 0.0386	0.9995	0.0005
	Awake	0.4726 ± 0.0464	HV	0.5975 ± 0.0125	0.9905	0.0095
	N-REM	0.5623 ± 0.0386	HV	0.5975 ± 0.0125	0.7999	0.2001

The cortical connectivity, estimated via the PTE algorithm, enabled the most significant discrimination between all the epochs. As shown in Table 4, the PTE was minimized during the ictal transition (0.8692), took higher values during the awake status (0.9063), was even higher during the N-REM period (0.9239), and was maximized during the HV maneuver (0.9399). In this case, the statistical test led to significant results even with a significance level of $\alpha < 0.01$. Besides showing the lowest median connectivity, the ictal transition reported the highest values in terms of the interquartile range. On the other hand, the HV and the N-REM epochs presented very similar interquartile ranges (≈0.152), lower than the ictal transition (0.1773) but higher than the awake periods (0.1305). Hence, the connectivity increment during the N-REM and HV phases was also associated with a higher variability, which goes against what was observed during the seizure onset. A visual representation of the overall results is given in Figure 2

Table 4. Comparison of the median and inter-quartile range of the Phase Transfer Entropy (PTE) computed in different groups of SEEG epochs.

Metric	Group 1		Group 2		*p*-Value	
	Label	Mean ± CI	Label	Mean ± CI	Greater	Less
$Med[PTE]$	Ictal	0.8692 ± 0.01976	Awake	0.9063 ± 0.0056	0.9922	0.0078
	Ictal	0.8692 ± 0.01976	N-REM	0.9239 ± 0.0057	0.9992	0.0008
	Ictal	0.8692 ± 0.01976	HV	0.9399 ± 0.0045	0.9999	0.0001
	Awake	0.9063 ± 0.0056	N-REM	0.9239 ± 0.0057	>0.9999	<0.0001
	Awake	0.9063 ± 0.0056	HV	0.9399 ± 0.0045	>0.9999	<0.0001
	N-REM	0.9239 ± 0.0057	HV	0.9399 ± 0.0045	>0.9999	<0.0001
$IQR[PTE]$	Ictal	0.1773 ± 0.0245	Awake	0.1305 ± 0.0046	0.0018	0.9982
	Ictal	0.1773 ± 0.0245	N-REM	0.1527 ± 0.0047	0.0461	0.9539
	Ictal	0.1773 ± 0.0245	HV	0.1522 ± 0.0053	0.0426	0.9574
	Awake	0.1305 ± 0.0046	N-REM	0.1527 ± 0.0047	>0.9999	<0.0001
	Awake	0.1305 ± 0.0046	HV	0.1522 ± 0.0053	0.9999	0.0001
	N-REM	0.1527 ± 0.0047	HV	0.1522 ± 0.0053	0.4360	0.5640

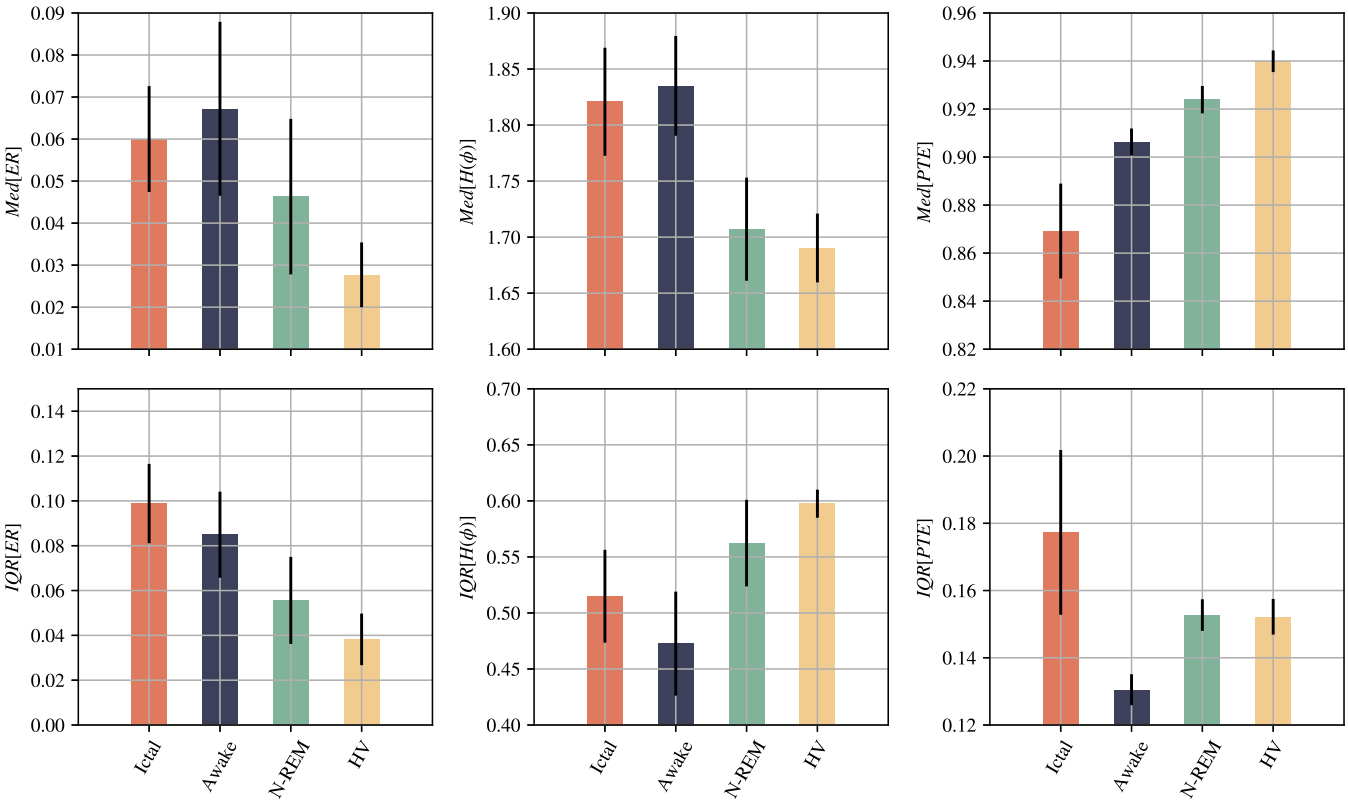

Figure 2. Comparison between the median and interquartile range of the analyzed metrics for the different groups of SEEG epochs; the top of each bar denotes the expected values, while the black vertical lines denote the confidence intervals.

5. Discussion

This is the first study to investigate HV using SEEG intracranial electrodes, offering novel insights into the impact of such a maneuver on the cortical brain signals. The results denote how HV shares similar characteristics in terms of energy ratio and phase entropy to N-REM sleep, and the same occurs for the awake status and ictal transition, where the latter includes the 20 s preceding and following the seizure onset. Specifically, ER and $H(\theta)$ are higher when the patient is conscious and during the ictal transition; in contrast, N-REM and HV present slower electrical activities, characterized by lower energy in high-frequency bands and more regular signal patterns. Interestingly, HV presents a reduced ER than awake status and, thus, seems to mitigate the rise in fast oscillations: this is in apparent contradiction to the scope of such an activation maneuver.

The low effectiveness of the energy ratio and the phase entropy in discerning HV from the N-REM status may be explained by the fact that such metrics do capture the interdependency between different cortical sites but analyze each signal as an independent element. More insights into HV are obtained by looking at the PTE, which, instead, enables full discrimination between all the SEEG groups. Particularly, the PTE algorithm captures the characteristics of intrasignal relationships across multiple frequency bands. This is very beneficial for analyzing epileptiform activities, which, notably, are not confined to specific frequency ranges but affect both fast and slow oscillations [28]. Our results show that HV increases the PTE, even more strongly than N-REM, while ictal transition behaves in the opposite fashion. This is in agreement with past studies that proved that the epileptogenic network presents reduced connectivity during the early ictal phase while being characterized by higher synchronization during seizure propagation. The ictal connectivity pattern may be explained by observing that the epileptogenic area adopts

a pathological behavior and, thus, results in being desynchronized by the rest of the network [29].

At first glance, our study denotes that HV is on the opposite side with respect to ictal transition, both in terms of the cortical connectivity and energy ratio, making its role in triggering seizures questionable. These findings are in line with other clinical studies on adults with focal epilepsy, suggesting that HV rarely triggers either clinical seizures or increases epileptiform discharges [10]. The connectivity increase during HV may be related to the specific characteristics of slow oscillations, which has been identified as a primary driver of interictal activity during N-REM sleep [30–32]. The cortical hypersynchronization has also been called into question to explain the IED diffusion that usually is observed in both N-REM sleep and HV, in opposite fashion with respect to the REM phase in which the IEDs becomes more focused [32,33]. The fact that HV replicates the N-REM patterns explains the effectiveness of this activation maneuver in generalized epilepsy, such as absence epilepsy, where IED exploits the burst-firing mode of the wide-projecting corticothalamic system as is well documented during N-REM sleep [30].

The fact that cortical brain regions during HV replicate the conditions observed during the N-REM status has been hypothesized by some previous studies but, to our knowledge, was never shown via intracranial EEG recordings. This may steer against the current clinical practices, which recommend the use ofHV as an activation maneuver for both generalized and focal epilepsy. One could speculate that HV promotes a conductive environment that facilitates seizure propagation in focal epilepsy, but such an effect is not sufficient to trigger the seizure onset. In our experience during long-term EEG and SEEG monitoring, we have rarely observed seizures during such a procedure in the case of focal epilepsy: in some cases, seizures developed only after several HV sessions or minutes after the activation maneuver was carried out. This may suggest that the transition from a state of increased connectivity to a state with relatively decreased connectivity facilitates the focal desynchronization of epileptogenic sites and the consecutive rise in ictal discharges.

It is noteworthy that the EZ, namely, the cortex area responsible for seizure generation, responds differently to the HV maneuver compared to healthy cortical and subcortical regions. A past study demonstrated that, during HV, the mean decreases in cerebral blood flow were 20.9% and 10.8%, in epileptic and non-epileptic temporal cortical regions, respectively [5]. The authors found a linear dependency between the blood flow reduction and the interval between seizures, concluding that the EZ is more susceptible to hypoperfusion and particularly vulnerable to ischemia. Even if HV exerts a global connectivity effect, different pathological and physiological areas may respond in a personalized fashion. Therefore, studying how HV affects the cortical sites within the EZ may enable the definition of new biomarkers for better EZ localization.

Our study has several limitations. First, the sample size was limited and heterogeneous in terms of etiology and explored cortical areas, though most patients had a temporal EZ and exploration focused mainly on temporal structures. Further validation of our findings over a broader population with uniform characteristics represents an essential step for continuing this research and its effectiveness from a clinical point of view. Secondly, we did not systematically assess the relative increase or decrease in IED frequency during N-REM sleep, wakefulness, and HV periods, which could be either a cause or effect of the observed connectivity changes. Additionally, due to the small sample size, we did not separately analyze patients in whom HV induced IED versus those in whom the maneuver had no effect. From a methodological point of view, we considered only the PTE algorithm for estimating cortical connectivity, while extending the analysis by considering frequency-dependent metrics may enable discerning connectivity patterns according to specific frequency bands. We did not assess connectivity changes within the EZ compared to propagation zones, unaffected zones, and contralateral healthy control areas. Lastly, SEEG explorations are only conducted in people with drug-resistant epilepsy, as the invasive nature of the procedure precludes the inclusion of healthy control subjects.

6. Conclusions

In this work, we studied the effects of HV on cortical brain structures of 10 patients with drug-resistant focal epilepsy who underwent SEEG monitoring. We exploited different quantitative metrics to analyze the intracranial signals, considering the PTE algorithm to estimate the effective connectivity between the cortical sites explored by the SEEG implants. We observed that HV strongly increases cortical connectivity in focal fronto-temporal epilepsy, similar to what occurs during N-REM sleep. While HV may induce a conductive environment that facilitates the propagation of epileptiform activity, it seems insufficient to trigger seizure development, contrary to what occurs in generalized epilepsy. Hence, our findings suggest that HV should be considered a facilitating maneuver rather than an activation procedure. At the same time, analyzing the specific connectivity behavior of epileptogenic versus healthy areas during the HV maneuver could provide useful information for identifying new biomarkers that characterize the EZ.

Author Contributions: Conceptualization, L.F., F.M., M.M. and F.B.; Formal analysis, L.F. and F.M.; Investigation, L.F., F.M., L.D.V., E.P., R.M. (Roberto Michelucci), M.M. and F.B.; Methodology, L.F. and F.M.; Supervision, M.M. and F.B.; Writing—original draft, L.F. and F.M.; Writing—review and editing, L.F., F.M., L.D.V., E.P., R.M. (Roberto Michelucci), F.C., R.M. (Roberto Mai), L.A., L.Z., M.M. and F.B. All authors have read and agreed to the published version of the manuscript.

Funding: This research received no external funding.

Institutional Review Board Statement: The study was conducted in accordance with the Declaration of Helsinki. The study received approval from the Central Emilia Wide Area Ethical Committee of the Emilia-Romagna Region (protocol number 89-2021; committee code 20230)

Informed Consent Statement: Written informed consent was obtained from each patient participating in the study.

Data Availability Statement: The datasets presented in this article cannot be shared according to the approved Istitutional Review Board. Requests to access the datasets should be directed to the corresponding author.

Conflicts of Interest: The authors declare no conflicts of interest.

References

1. Kane, N.; Grocott, L.; Kandler, R.; Lawrence, S.; Pang, C. Hyperventilation during electroencephalography: Safety and efficacy. *Seizure* **2014**, *23*, 129–134. [CrossRef] [PubMed]
2. Foerster, O. Zur Pathogenese und chirurgischen Behandlung der Epilepsie. *Zentralbl Chir* **1925**, *52*, 531–549.
3. Gibbs, F.A.; Lennox, W.G.; Gibbs, E.L. The electro-encephalogram in diagnosis and in localization of epileptic seizures. *AMA Arch. Neurol. Psychiatry* **1936**, *36*, 1225–1235. [CrossRef]
4. Siddiqui, S.R.; Zafar, A.; Khan, F.S.; Shaheen, M. Effect of hyperventilation on electroencephalographic activity. *J. Pak. Med. Assoc.* **2011**, *61*, 850–852. [PubMed]
5. Weinand, M.E.; Carter, L.P.; Oommen, K.J.; Hutzler, R.; Labiner, D.M.; Talwar, D.; El-Saadany, W.; Ahern, G.L. Response of human epileptic temporal lobe cortical blood flow to hyperventilation. *Epilepsy Res.* **1995**, *21*, 221–226. [CrossRef] [PubMed]
6. John, W.; Wang, S. Response of medullary respiratory neurons to hypercapnia and isocapnic hypoxia. *J. Appl. Physiol.* **1977**, *43*, 812–821. [CrossRef]
7. Assenza, G.; Mecarelli, O.; Tombini, M.; Pulitano, P.; Pellegrino, G.; Benvenga, A.; Assenza, F.; Campana, C.; Di Pino, G.; Di Lazzaro, V. Hyperventilation induces sympathetic overactivation in mesial temporal epilepsy. *Epilepsy Res.* **2015**, *110*, 221–227. [CrossRef]
8. Rana, M.; Steenari, M.; Shrey, D. Hyperventilation and Seizures: Not a New sense: A Literature review. *Neuropediatrics* **2023**, *54*, 359–364. [CrossRef]
9. Mason, F.; Scarabello, A.; Taruffi, L.; Pasini, E.; Calandra-Buonaura, G.; Vignatelli, L.; Bisulli, F. Heart Rate Variability as a Tool for Seizure Prediction: A Scoping Review. *J. Clin. Med.* **2024**, *13*, 747. [CrossRef]
10. Holmes, M.D.; Dewaraja, A.S.; Vanhatalo, S. Does hyperventilation elicit epileptic seizures? *Epilepsia* **2004**, *45*, 618–620. [CrossRef]
11. Guaranha, M.S.; Garzon, E.; Buchpiguel, C.A.; Tazima, S.; Yacubian, E.M.; Sakamoto, A.C. Hyperventilation revisited: Physiological effects and efficacy on focal seizure activation in the era of video-EEG monitoring. *Epilepsia* **2005**, *46*, 69–75. [CrossRef] [PubMed]
12. Li, Z.; Hwang, K.; Li, K.; Wu, J.; Ji, T. Graph-generative neural network for EEG-based epileptic seizure detection via discovery of dynamic brain functional connectivity. *Sci. Rep.* **2022**, *12*, 18998. [CrossRef] [PubMed]

13. Sakkalis, V. Review of advanced techniques for the estimation of brain connectivity measured with EEG/MEG. *Comput. Biol. Med.* **2011**, *41*, 1110–1117. [CrossRef]
14. Lobier, M.; Siebenhühner, F.; Palva, S.; Palva, J.M. Phase transfer entropy: A novel phase-based measure for directed connectivity in networks coupled by oscillatory interactions. *Neuroimage* **2014**, *85*, 853–872. [CrossRef]
15. Mazzucchi, E.; Vollono, C.; Losurdo, A.; Testani, E.; Gnoni, V.; Di Blasi, C.; Giannantoni, N.M.; Lapenta, L.; Brunetti, V.; Della Marca, G. Hyperventilation in Patients With Focal Epilepsy: Electromagnetic Tomography, Functional Connectivity and Graph Theory—A Possible Tool in Epilepsy Diagnosis? *J. Clin. Neurophysiol.* **2017**, *34*, 92–99. [CrossRef]
16. Mercier, M.R.; Dubarry, A.S.; Tadel, F.; Avanzini, P.; Axmacher, N.; Cellier, D.; Del Vecchio, M.; Hamilton, L.S.; Hermes, D.; Kahana, M.J.; et al. Advances in human intracranial electroencephalography research, guidelines and good practices. *Neuroimage* **2022**, *260*, 119438. [CrossRef] [PubMed]
17. Talairach, J.; Bancaud, J. Lesion, "irritative" zone and epileptogenic focus. *Ster. Funct. Neurosurg.* **1966**, *27*, 91–94. [CrossRef]
18. Cardinale, F.; Cossu, M.; Castana, L.; Casaceli, G.; Schiariti, M.P.; Miserocchi, A.; Fuschillo, D.; Moscato, A.; Caborni, C.; Arnulfo, G.; et al. Stereoelectroencephalography: Surgical methodology, safety, and stereotactic application accuracy in 500 procedures. *Neurosurgery* **2013**, *72*, 353–366. [CrossRef]
19. Greene, P.; Li, A.; González-Martínez, J.; Sarma, S.V. Classification of stereo-EEG contacts in white matter vs. Gray matter using recorded activity. *Front. Neurol.* **2021**, *11*, 605696. [CrossRef]
20. Pigeau, R.; Hoffmann, R.; Moffitt, A. A multivariate comparison between two EEG analysis techniques: Period analysis and fast Fourier transform. *Electroencephalogr. Clin. Neurophysiol.* **1981**, *52*, 656–658. [CrossRef]
21. Bartolomei, F.; Chauvel, P.; Wendling, F. Epileptogenicity of brain structures in human temporal lobe epilepsy: A quantified study from intracerebral EEG. *Brain* **2008**, *131*, 1818–1830. [CrossRef] [PubMed]
22. Scott, D.W. Sturges' rule. *Wiley Interdiscip. Rev. Comput. Stat.* **2009**, *1*, 303–306. [CrossRef]
23. Chua, K.; Chandran, V.; Rajendra Acharya, U.; Lim, C. Analysis of epileptic EEG signals using higher order spectra. *J. Med. Eng. Technol.* **2009**, *33*, 42–50. [CrossRef] [PubMed]
24. De Clercq, W.; Lemmerling, P.; Van Paesschen, W.; Van Huffel, S. Characterization of interictal and ictal scalp EEG signals with the Hilbert transform. In Proceedings of the 25th Annual International Conference of the IEEE Engineering in Medicine and Biology Society, Cancún, Mexico, 17–21 September 2003; Volume 3, pp. 2459–2462.
25. Chiarion, G.; Sparacino, L.; Antonacci, Y.; Faes, L.; Mesin, L. Connectivity analysis in EEG data: A tutorial review of the state of the art and emerging trends. *Bioengineering* **2023**, *10*, 372. [CrossRef] [PubMed]
26. Friston, K.J. Functional and effective connectivity in neuroimaging: A synthesis. *Hum. Brain Mapp.* **1994**, *2*, 56–78. [CrossRef]
27. West, R.M. Best practice in statistics: Use the Welch t-test when testing the difference between two groups. *Ann. Clin. Biochem.* **2021**, *58*, 267–269. [CrossRef]
28. Edakawa, K.; Yanagisawa, T.; Kishima, H.; Fukuma, R.; Oshino, S.; Khoo, H.M.; Kobayashi, M.; Tanaka, M.; Yoshimine, T. Detection of epileptic seizures using phase–amplitude coupling in intracranial electroencephalography. *Sci. Rep.* **2016**, *6*, 25422. [CrossRef]
29. Mason, F.; Ferri, L.; Vito, L.D.; Alvisi, L.; Zanuttini, L.; Martinoni, M.; Mai, R.; Cardinale, F.; Tinuper, P.; Michelucci, R.; et al. Desynchronization Index: A New Approach for Exploring Complex Epileptogenic Networks in Stereoelectroencephalography, *arXiv* **2024**, arXiv: 2408.16347.
30. Nobili, L.; Frauscher, B.; Eriksson, S.; Gibbs, S.A.; Halasz, P.; Lambert, I.; Manni, R.; Peter-Derex, L.; Proserpio, P.; Provini, F.; et al. Sleep and epilepsy: A snapshot of knowledge and future research lines. *J. Sleep Res.* **2022**, *31*, e13622. [CrossRef]
31. Steriade, M. Grouping of brain rhythms in corticothalamic systems. *Neuroscience* **2006**, *137*, 1087–1106. [CrossRef]
32. Frauscher, B.; von Ellenrieder, N.; Ferrari-Marinho, T.; Avoli, M.; Dubeau, F.; Gotman, J. Facilitation of epileptic activity during sleep is mediated by high amplitude slow waves. *Brain* **2015**, *138*, 1629–1641. [CrossRef] [PubMed]
33. Sammaritano, M.; Gigli, G.L.; Gotman, J. Interictal spiking during wakefulness and sleep and the localization of foci in temporal lobe epilepsy. *Neurology* **1991**, *41*, 290–290. [CrossRef] [PubMed]